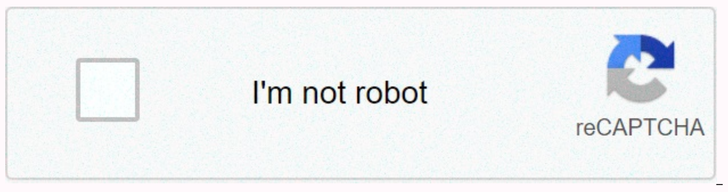


Continue

# Snmmi procedure guidelines for myocardial perfusion imaging

This section describes the purchase protocols for spect/CT MPI, PET/CT MPI, 18F-FDG PET/CT, cardiac CT, and radionuclide and CT merge images. Visualization of SPECT/CT MPI perfusion can be performed using 99mTc or 201Tl agents using previously described protocols (5). SPECT is standard, with planar imaging limited to the imaging of claustrophobic patients and patients with high body content (patients above the weight limit of the image table or unable to fit within the scanner's gantry). Closed SPECT is recommended whenever possible. For 99mTc, the most commonly used protocols are 1-d, low rest dose and high-dose stress protocol (Table 3) or 2-d protocol (for patients with high body mass index) with equal radiotractor injection (925-1,110 MBq [25-30 mCi] 99mTc) (5). A protocol using 201Tl in the rest and 99mTc perfusion tracers during stress, the so-called dual isotope technique, allows for a shorter study, but due to a higher dose of radiation.201Tl MPI with 4- and 24-h redistributive imaging is also used to assess the viability of myocardium. If the 99mTc isotope is not available, 201Tl is an alternative agent for MPI rest and stress. Stress-only imaging with 99mTc can reduce test duration, dose and radiation costs. Preliminary evidence suggests that normal STRESS-only SPECT is equivalent to normal rest and MPI stress to stratify risk in low-risk patients (34.35). Stress-only MPI may be seen as an option by experienced and well-qualified doctors in highly qualified low-risk or very low-risk patients when stress images are expected to be normal (36). The default SPECT protocol is displayed in Table 3 (5). Patients are scanned by lying (standard), prone (optional) or vertical depending on local preferences and scanner type. SPECT/CT often uses an acquisition protocol that has a 128-× 128 matrix with a zoom factor of 1.0. The CT protocols for SPECT/CT and PET/CT are described in part E4 of this section (5). PET/CT MPI MPI (13N-ammonia or 82Rb) and myocardial metabolic imaging (18F-FDG) can be performed using PET (6). Previously, details of 13N-ammonia imaging protocols (6) were published. 82Rb is the most commonly used radiotracker for PET MPI. Patients are usually scanned lying down with their arms raised above their shoulders. The position of the heart is localized using a scouting CT image (10 mA, 120 kV), followed by CTAC (10-20 mA, 120 kV) for emissions correction and visualization. For 82Rb, 1,480–2,040 MBq (40–60 mCi) (2-th), 370–740 MBq (10–20 mCi) (3- measuring, vismuth of germanic systems), or 1110-1480 MBq (30-40 mCi) (3-throttle, lut of ocsyorthosilikatic systems) are introduced and then purchased for 7 minutes without delaying the prescan using list mode (preferably), or in closed or static mode using delays (70-90 s for left stomach ejection fraction > 50% and 91-130 s for left stomach ejection fraction < 50%). Stress testing (mainly pharmacological stress) stress) the use of standard protocols and radiotracters administered with maximum hyperemism, followed by the same rendering steps as described for MPI rest. Exercise stress isn't often used, but it's possible with 13N-ammonia and complex with 82Rb. Typically, a patient's position doesn't change on the scanner table between others and stressful images, and one CTAC study is adequate for correcting the formwork of the rest and stressful images. If a patient moves after resting MPI, CTAC after MPI stress may be preferable to CTAC during peak hyperemia, especially when using vasodilator stress due to respiratory stimulation caused by vasodilator agents. List-mode emissions data is not counted in closed, static, and dynamic image sets for analysis. Images are reconstructed using filtered reverse production or iterative expectation maximization (e.g. maximum waiting for ordered subsets). Cardiac PET protocols have been described in detail before (Table 4) (6). Visualization of 18F-FDG PET/CT Cardiac 18F-FDG is performed to assess the viability of the myocardial and detect heart inflammation (e.g., sarcoidosis). To assess the viability of the myocardium, you can follow these steps: Perform other MPI using 82Rb or 13N ammonia as described above for PET/CT MPI. Some facilities use MPI fixed by SPECT/CT, or a closed SPECT MPI study to compare with an 18F-FDG study. Follow this by loading glucose and administering insulin to assess viability using standard protocols (6). Check your baseline blood sugar and follow glucose loading protocols in or intravenously, as shown in Tables 5 and 6 (6). Perform 18F-FDG visualization as a closed study (if possible) for 15-30 minutes using the previously described parameters (Table 7). In the case of high activity in the blood pool in 18F-FDG images (insulin resistance is usually observed), more intravenous insulin may be prescribed and images (6) may be reused. 18F-FDG imaging is performed to assess myocardial inflammation in patients with suspected or known cardiac sarcoidosis (37–40). Previous retrospective studies suggest high accuracy and superiority compared to 67Ga visualization (38). Fasting imaging of 18F-FDG can lead to variable myocardial glucose physiological intake. Thus, to ensure absorption of inflamed tissue, but to optimize the inhibition of 18F-FDG absorption by normal mocytes (reduce nonspecific absorption), patients are instructed to take a diet, fat-free for 12-24 hours before the test or quickly for 12-18 hours and/or use intravenous heparin, 15-50 units/kg, about 15 minutes before injection of 18F-FDG (40.41). Initially, another MPI (SPECT or PET) study is conducted, preferably a closed scan). This is followed by intravenous administration of 18F-FDG (370-555 MBq mCi]), a 90 min absorption period and subsequent purchase of static images using the parameters described in Table 7. Visualization of the entire body of 18F-FDG is performed from the cerem to the upper thigh to be to assess 18F-FDG absorption in extracardiac regions (neck, mediastinal, lungs, and abdominal lymph nodes). The remaining myocardial performances and cardiac 18F-FDG images are reconstructed and refocused on standard heart planes (short axis, vertical long axis and horizontal long axis) for interpretation. Images of 18F-FDG of the whole body should be interpreted by trained nuclear medicine physicians or doctors who have credentials to monitor and interpret the body's pet/CT (42.43). Computed tomography of atenu-correction (CTAC) For hybrid imaging procedures, three types of CT protocols are used: non-heating, non-released, free computer tomography of tinged breathing (thickness of slices 5 mm) for potency correction; uncapped, closed, breathable computer scanning (2 to 3 mm thick) for coronary artery calcium; and contrasting, closed, respiratory CT (slice thickness from 0.5 to 0.75 mm) for coronary CTA. A few years ago, a CT scan was incorporated into hybrid devices solely for the purpose of itutation correction (44). The main advantage of these initial devices was that the CT image had a low time and spatial resolution and is more comparable to the resolution of radionuclide scans, and can lead to fewer artifacts incorrectly registering. However, the duration of the scan was extended, and limited CT scans were not useful for localizing anatomical diseases, especially for common applications of nuclear medicine. Subsequently, diagnostic CT scanners (2-, 4-, 6-, 8-and 64-th CT scans with multidetectors) were integrated with spectrat or PET scanners, which allowed to quickly obtain standard multi-detector CT scans for correction of intensity, calcium cinging of coronary artery and coronary TTA. These scanners produce high-resolution CT scans of approximately 10 s. Due to faster imaging in relation to emissions scanning, heart position is averaged over several breath cycles, compared to SPECT or PET, for which the heart position averages more than 5-12 minutes (6). This has led to a relatively higher frequency of improper registration of artifacts and the need to consider various protocols for coregister PET (or SPECT) and CT images. Researchers experimented with a variety of breathing methods, such as free tingling, holding your breath at the end of inspiration or holding your breath at the end of term (45). Currently, free watering breathing with airway averaging appears to be the best technique (6). Low doses or ultra-low CT doses (46.47), as well as slow CT scans (48.49) and ultra-fast CT scans, have attempted to match image resolution with MPI in an attempt to improve mpi and CT image registration, but without clear benefits. Double closed PET/CT with ECG-thyr and pecking for respiratory movements are possible and checked (50-52). Some new generation rapid SPECT scanners have a low dose of CT correction (53). recommendations for CT transmission visualization are listed in Table 8. Scanning transmission with shallow tidying is the best protocol. The current of the tube and voltage of approximately 10-20 mA and 80-140 kVP are recommended. For PET MPI, one CTAC is standard (since a patient can undergo a stress agent in a PET horse). However, due to patients' frequent movements between individually acquired MPI and CTAC studies, which can be difficult to detect by patient observation, or if the patient moves between the rest and MPI stress, a separate ANTAC can be used for the rest and MPI stress studies (optional). Some scanners would not allow CTAC to be used to correct potency if the patient's position or table shifted by more than 5mm between transmission and emission imaging. For SPECT MPI, separate computed tomography is usually required for the rest and stressful MPI research. The use of CT transmission to assess coronary artery calcium may roughly estimate the extent of coronary calcification (54). This approach, however, does not provide an accurate measure of coronary artery calcium, as it is an inhositical study that has artifacts due to the movement of coronary arteries. In addition, scanning attenuation comes with a much lower photon density than scanning the calcium score. Often, the use of KTA for visual evaluation of coronary artery calcium may not reveal a small amount of calcium in approximately 8% of patients (54). The use of calcium CT scan of coronary artery for correction of ignization (55.56) was investigated. However, calcium assessment is the ultimate diastolic image obtained normally during breathing and cannot adequately register at MPI, which is a conjured image of the heart within several cardiac cycles obtained during shallow tivy breathing. Coronary artery calcium scans of coronary artery CT of coronary artery calcium are performed according to standard protocols as described above (28). Scanners with excellent spacious and temporary resolution should be used to ensure good image quality (see section VIII, Equipment Specification) (13.28). Unpinned, prospective axial acquisition caused by ECG is reconstructed at a cut thickness of 2.5 or 3 mm at 65%-80% of the R-R cycle during the breathing pyritic. To reduce radiation dose, the use of promising triggering (depending on the type of scanner) (56.57) may be useful, with the X-ray tube activated only in the specified phase of the heart cycle (as opposed to the retrospective weight), thereby reducing the dose delivered to the patient. Although, in theory, imaging parameters can be adjusted based on the body's habit for reducing radiation dose (reducing tube current or voltage in patients with a lower body mass index), only the standard tube potential (kVp) and current (mA) settings are currently recommended for accurate coronary artery calcium clogging. Preliminary evidence suggests that the tube's potential of 100 kVP can reliably measure coronary artery calcium; however, the approach requires a different calcium threshold of 130 HU, which algorithms for assessing calcium and may vary depending on the scanners. Despite potential use in reducing radiation dose, the use of lower tube potential has yet to be confirmed, and no standard threshold has been set for coronary artery calcium clogged (58). Retrospective heliium imaging is not expected due to the increased radiation load on the patient. A promisingly triggered no-overlapping snippets mode (step and take-off acquisition) has been shown to reduce the radiation dose significantly, compared to the ferocious overlapping image mode (29.59). High heart rates can impair image quality. However β are not used before scanning coronary artery calcium. The coronary FTA listed below are proposed recommendations for the effectiveness of the coronary FTA; however, these parameters and recommendations may vary depending on the patient's heart output, heart rate and rhythm, as well as the type of scanner, supplier, and platform). Some technical considerations for CTA and MPI hybrid coronary studies should be considered. Scanners used must have excellent space and temporary resolution to ensure image quality (see section VIII, Equipment specifications) (13,28,29). Patient training. For the study of coronary FTA requires a large needle (for the rapid introduction of iodineous contrast material at 4-7 ml/min), ideally in an anti-cubital foss. The wrist should be avoided because of the risk of extravasion. If the study is planned as a combined study with rest and stress mpi, it is better to perform an MPI scan before CT scan (to minimize any potential obstacles in correcting ionization from iodized contrast material). For pharmacological studies, the stress vasodilator prefers stress extraction due to increased heart rate from infusion of doutamine. U.S. or β blockers are commonly used before coronary FTA to bring heart rate to a target of 50-60 bpm. Because the temporary resolution of the scanners is limited, motion artifacts are minimized at a heart rate of less than 60 bpm. β-blocker may be less commonly needed when dual-source CT technology of higher temporal resolution enters hybrid scanners. Nitroglycerin (0.4 mg sublingual or 1 spray) is often used immediately before coronary FTA research to improve visualization of smaller-caliber coronary vessels through vasodilation). It is advisable to iodine contrasting material with a maximum concentration of iodine vasodilation (≥300 mg I/ml). Whether isosomolar contrast agents surpass more osmolar contrast material for nephrotoxitic prevention is still a matter of debate. Contrast material is injected intravenously at a speed of 4-7 ml/s. The amount of contrast material used varies (50–120 mL) based on the selected speed z-dimension scanning length, scanner type, and selected scanning mode (retrospectively ECG-closed, promising triggering or a promisingly triggered high-pitch spiral scan mode). Technical details. Coronary CTA scanning on hybrid devices is acquired according to standard protocols (13,28,29). To reduce the radiation dose, it is important to adjust the dose based on the body's habit. Reducing the potential of a tube from 120 kV to 100 kV should be considered in individuals weighing less than 85 kg or having a body mass index of less than 30 kg/m2, and a reduction of up to 80 kV can be considered in thinner patients (60). Higher tube current and voltage can be seen in people with obesity to improve signal to noise ratio. Ecg dose modulation with low current tube during systholitic phases (28,29,60) is recommended when using retrospective hewning. Promising methods are triggered to reduce the radiation dose (59.61.62). Instead of a low helic mode pitch with overlapping images, a promising ECG-induced scan

using axial (step and shooting) acquisitions can significantly reduce the dose while maintaining image quality (62.63). This approach applies only when the patient's heart rate is slow enough (<60 bpm) and there is no arrhythmy. Expanding the purchase window (filling) (interval when activating the X-ray tube) must be minimized to keep a low radiation dose (64). Promising triggering overshadows the possibility of evaluating LV function using closed CT methods. New methods to further minimize radiation dose from coronary TTA using prospective purchase of high-pitch spiral (65) or adaptive statistical iteration reconstruction algorithms (66.67). To optimize the duration of scanning using hybrid 82Rb PET/CTA, the first stress protocol with vasodilator stress may be considered. β-blockers can be administered intravenously (metoprolol, 5mg, repeated at 5-minute intervals) after 82Rb MPI stress is completed. Coronary steps of the FTA (13.28.29). Each step in the coronary DAC is performed using breathing instructions to train the patient. A chest scouting check is carried out to localize the heart position. This scan can be used to determine the starting and final locations for coronavirus CTA research. Coronary CTA scan length ranges from 2.5 to 5.0 cm above the main takeoff of the aorta and 2.5 to 5.0 cm below the bottom of the heart silhouette determined by the scout's image. Since the duration of the scan determines the duration of breathing retention and the dose of radiation to patients, the minimum required scan length should be used. However, if the scan length is too tight, there is a risk of not turning on the takeoff of the left major coronary artery or the dystal posterior lower arteries. Often the carina is used as a cranial landmark because it is easily identified in the topographical image of the scout and avoids the risk of the left main or left front descending coronary The arrival of contrasting material in the ascending aorta is learned by scanning the pain of time or purchasing a bolus to automatically trigger the scan. Scan. scanning of the bolus during timing, 10-20 ml of iodized contrast material is administered at 4-6 ml/s using a power injector, followed by approximately 20 ml of conventional saline chase. Scanning started (10 s later) as one CT slice 2 cm above the aorta root, 1 image every 2 s. Aorta is observed by contrasting opacity, and the acquisition stops when there is a decrease in opacity. Images are viewed visually (optionally) or using an application (standard) to identify a snippet with maximum contrast and calculate time to peak opacity (including 10s delay). Once the peak time of opacity contrast in the aorta is determined, an additional 3-4 s is added to allow the opacity of the coronary arteries. This procedure offers the benefits of testing the intravenous line, avoids the risk of delay or early onset of imaging, and provides an opportunity to monitor the patient's cooperation with instructions and breathing (28). Acquiring bolus tracking for automatic scanning is based on a given intensity of increasing contrast in the ascending or descending aorta (e.g. 100 HU). In this mode, the gantry is stationary and performs repeated axial scans through the aorta. The CTA acquisition is triggered when the region of interest over the aorta achieves a given increase in contrast. The two-camera power injector is loaded with contrast in one eclusion and a normal saline solution in another. Typical contrast injection rates range from 4 to 7 mL/s, dependent on body habit and cardiac output. Higher rates of 7-8 mL can sometimes be used in people with high cardiac output. Typically, 50-120 ml of contrasting material is injected with about 40-ml of normal saline washing during breathing. The exact amount of contrast material is based on the duration of the scan (which is based on the set start and end locations) and other parameters as described above. Saline chase is used to keep dense blyus of contrasting material and clean the material from the right heart to avoid a band of artifacts on the right coronary artery. The images are reconstructed using the standard parameters to the thinnest possible fragment (0.5–0.75 mm, determined by the scanner detector configuration), in increments that will overlap approximately a third of the fragment (improves the resolution in the z-dimension). In patients with a high body mass index, a slightly thicker slice (1 mm) can be used to avoid images with poor signal to noise ratio. Scanners with editing capabilities can use ECG editing to improve cardiac movement from accidental ectopic shock during purchase. Images can be reconstructed in a wider field of view to study and interpret extracardiac results. Fusion of radionuclide and CT images of Radionuclide and CT images are acquired and can be displayed separately or as a flatted image (overlay of radionuclide and CT images) using or software methods. Images are not acquired in merged mode. Management decisions are usually made through integrated diagnostic information from radionuclide (SPECT or PET) and CT scans without actually merging images, as well as merged images. Page 2 ImmunoPET Status: Wright and Lapy provide a brief overview of the use of positron-emitted isotopes in tracking and visualizing the localization of monoclonal antibodies and discussing the advancement of these technologies into clinical use. Page 1171 Tumor Hypoxia Imaging in NSCLC: Bollinen and colleagues look at the potential added clinical value of a specific tracer of hypoxia 18F-phthorazomacin arabinosiside over 18F-FDG in assessing treatment for non-cell lung cancer. Page 1175 11C-tariquidar/11C elacridar in humans: Bauer and colleagues examine the suitability of these 2 radiolablain P-glycoproteins and breast cancer resistance protein inhibitors to assess pet density of P-glycoprotein in the human brain. Page 1181 Response quantification with SUV metrics: Vanderhoek and colleagues examine the impact of various standardized cost consumption measures on the quantification and classification of PET-based treatment response. Page 1188 PET and Prostate Cancer Survival: Jadwar and colleagues correlate parameters derived from basic 18F-FDG PET/CT with overall survival in men with castrate-resistant metastatic prostate cancer and discuss the implications for comparing efficacy in treatment strategies. Page 1195 Survival Prognosis after SIRT: Fendler and colleagues examine the metabolic parameters of 18F-FDG PET/CT in survival prognosis after selective internal radiotherapy in patients with liver metastasis from colorectal cancer. Page 1202 18F-FLT PET and FOLFOX Response: Hong and colleagues evaluate the use of 18F-FLT PET for early prediction of standard anatomical response and survival outcomes in patients with metastatic colorectal cancer who receive leukorcin, 5-fluorouracil, and oxalipalin. Page 1209 18F-FET PET in Anti-Angiogenic Treatment: Heinzel and colleagues assess the clinical utility and cost-effectiveness of adding 18F-FET PET to MR structural imaging in the management of high-grade recurrent gliom treated with bucizumab and irinothecan. Page 1217 pet in Merkel's cell staging: Siv and colleagues determine the impact of 18F-FDG PET on prognostic stratification and management of Merkel's cell carcinoma. Page 1223 PET/CT and 131I therapy: Lee and colleagues look at the clinical benefit of 18F-FDG PET/CT, which is performed simultaneously with 131I therapy in patients with differentiated thyroid carcinoma and intermediate-high risk of recurrence. Page 1230 UR, PET and children's brain tumors: Chukotynsky and colleagues describe pet registration method with IMAGES of MR permeability to correlate 18F-FDG absorption, permeability and cerebral blood volumes in pediatric tumors brain and compare these results Results. Page 1237 Bone Marrow Lesion Imaging in DLBCL: Berthe and colleagues compare 18F-FDG PET/CT and bone marrow biopsy to detect bone marrow involvement in patients with newly discovered diffuse large B-cell lymphoma. Page 1244 SPECT and Professional Radiation: Duval and colleagues assess the effects of changes in stressful myocardial perfusion imaging protocols and highly effective SPECT camera technology in reducing professional radiation in the nuclear cardiology laboratory. Page 1251 pet and MVO2: Wong and colleagues determine whether PET 11C acetate can be used to quantify myocardial oxygen consumption in hypertrophied right ventilation in patients with idiopathic pulmonary arterial hypertension. Page 1258 GABA-A Imaging Receptor in Cerebral Palsy: Park and colleagues use 18F-fluoroflumazenil PET to investigate changes in γ-aminobutic acid-Receptor binding and functional and anatomical communication in the motor cortex in children with hemiplegic cerebral palsy. Page 1263 18F-FMZ PET for epilepsy: Vivash and colleagues report the results of phase I/IIa clinical use of 18F-FMZ PET to localize epileptogenic zones in patients with temporal lobe epilepsy. Page 1270 Of The Olterminal Tract and Cortical Metabolism: Cross and colleagues use 18F-FDG PET and diffusion tenzor imaging to investigate the relationship between the integrity of the fi booked tract in the olhatal tract with cork glucose metabolism in cognitively normal control and individuals with mild cognitive impairment. Page 1278 Kinetic Simulation 18F-JNJ-42259152: Van Laere and colleagues detail the initial kinetic brain simulation of this novel phosphodiesterase-10A PET tracer and evaluate the reproducibility of test-retretching in healthy volunteers. Page 1285 99mTc-MAA distribution and 90Y microspheres: Wondergem and colleagues determine the pre-therapy value of 99mTc-macroagregated albumin SPECT in the forecast of the final distribution of activity in 90Y-microperic radioembolization for primary or metastatic malignant liver diseases. Page 1294 11C-ITMM PET in humans: Toyohara and colleagues report safety, distribution, radiation dosmetrium and initial imaging of this agent to display type 1 metabolic glutamate receptor in the brain. Page 1302 α4β2-nAChR Visualization: Wong and colleagues describe the safety, reliability of test-retecating and initial quantitative evaluation in people of 18F-AZAN, a new radiotracter that binds to nicotine acetylcholine receptors α4β2. Page 1308 Radioidized Antibodies VAP-1: Autio and colleagues evaluate the effectiveness of fully human monoclonal anti-vascular adhesion protein-1 antibodies in rabbits and discuss the clinical potential of imaging inflammation and for anti-inflammatory therapy. Page 1315 TSPO Genotyp and 11C-PBR28 SUV: Yoder and colleagues look at whether standardized absorption cost measurements in the brain of 11C-PBR28 PET imaging can distinguish between protein 18 kDa affinity phenotyps in humans. Page 1320 Skeletal Imaging Visualization SPECT/scocaler CT scan: Lormann and colleagues assess the effect of a high-resolution conical beam CT scan with flat panels on the interpretation of bone SPECT in peripheral skeleton diseases. Page 1323 Of Farmakokinetics of Conyugats (EH)3: Eder and colleagues provide biodisclosure data on ability (EH)3 to clean up the tag to improve the pharmacokinetic properties of peptide radiopharmaceutical drugs, with a focus on enhanced clearance from critical organs. Page 1327 Visualization of dopaminergic neurotransmission: Tash and Poepperl provide an educational update on nigrosthriatal dopamine terminal imaging, with a focus on SPECT performed with the presinaptic transporter dopamine ligand 123I-FP-CIT in patients with known or suspected parkinson's syndrome. Page 1331 18F-EF5 PET and Antihypoxic Therapy: Chitneni and colleagues evaluate the usefulness of 18F-EF5 PET imaging to monitor and predict tumor response to hypoxia activated prodrug SN30000 plus radiation treatment. Page 1339 Quantify cell-level activity: Chouin and colleagues present a method of quantifying ex vivo activity using a α-camera device that allows you to measure activity in tumor cells in very small biological structures, with the potential for small-scale dosimetry and targeted α therapy. Page 1347 PET imaging with 18F-FDM: Furumoto and colleagues describe a practical method of synthesis of this derivative mannosis and stereo camera 18F-FDG and offer additional biological evidence of its potential for tumor imaging. Page 1354 PET and Osteosarcoma: Campanile and colleagues characterize various phenotypes of pet osteosarcoma, comparing the absorption of 18F-FDG, 18F-FMISO and 18F fluoride in doclinic mouse models that reflect the heterogeneity of human disease. Page 1362 99mTc-PSMA inhibitors: Hillier and colleagues describe a preclinical assessment of 4 novel 99mTc-marking small molecules of prostate-specific membrane antigen inhibitors with the potential for molecular imaging of prostate cancer in humans. Page 1369 11C-SA4503 intake in pituitary gland tumors: Ramakrishnan and colleagues detail the kinetics of this PET tracer in the tumor and brain in rats to investigate its usefulness when transexpression of receptors σ-1 in pituitary tumors is detected. Page 1377 ARBs and 18F-FDG Absorption: Zhao and colleagues study the effects of angiotensin II receptor blockers on the distribution of 18F-FDG and excretion in mice treated telmisartan at various doses and discuss the implications for pet clinical practice. Page 1384 Pretargeted PET with click chemistry: Zeglis and colleagues report on the development of a pre-PET imaging methodology with the potential for high-quality images and dramatically reduced doses of non-targeted radiation for patients. Page 1389 Visualization of radiation damage: Johnson and colleagues describe the technique using a γ camera and a 99mTc-terracycline HCl to depict temporal and spatial distribution of damage in sensitive tissues after high-dose radiation. Page Page Intrauterine distribution 177Lu-mAbs: Erbom and colleagues examine the distribution of monoclonal antibodies 177Lu-DOTA-BR96, targeting Lewis Y antigen over 7 d using a syngeneic model of rat colon carcinoma. Page 1404 Testing model 18F-CPFPX: Elmenhorst and colleagues report on the development and evaluation of practical pharmacokinetic models to quantify the A1 adenosine receptor in high-resolution PET. Page 1411 18F-labeled tracers for τ visualization: Okamura and colleagues detail the development of an 18F-labeled novel derivatives of arylkinollin, 18F-THK-5105 and 18F-THK-5117, for use in PET imaging microtubule-related protein τ in neurofibrillation tangles in Alzheimer's disease. Page 1420 Ketamine and Binding 5-HT2A Receptors: Waelbers and colleagues use SPECT to investigate brain kinetics 123I-5-I-R91150, 5-HT2A receptor antagonist, and exposure to ketamine on post-serotonin-2A receptor status in cats. Page 1428 11C-PIB PET in Transgenic Mice: Snellman and colleagues evaluate the ability of 11C-Pittsburgh compound B PET to detect changes over time in β-amyloid deposits in the brains of 3 transgenic mouse models of Alzheimer's disease. Page 1434 SPECT Imaging VCAM-1: Dimastromatteo and colleagues are investigating the ability of twenty 99mTc-markings of the main complex of its composite 1-derivative peptide B2702p derivatives to facilitate the visualization of the vascular cell adhesion molecule 1 in an experimental model of atherosclerosis. Page 1442 NLD Systemic Gene Therapy: Grunwald and colleagues use sodium iodide symporter as a theranostic gene to investigate whether Adenovirus coating with synthetic dendrimers can be useful in developing adenovirus vectors for combination oncolytic virology and NIS mediatic radiotherapy. Page 1450 Visualization of GLP-1R in pancreas: Selvarajou and colleagues evaluate 68Ga-marking exendin-4 for PET imaging and quantification of glucagonlyca-like peptide 1 receptor-specific absor absor tissue absor vivo and discuss the implications for imaging native β cells. Page 1458 Phantom Fluids for PET/MRI: Ziegler and colleagues review and evaluate different approaches to fluid sampling for simultaneous PET/MRI phantom image. Page 1464 Responsive Template Registration: Lundqvist and colleagues suggest using a responsive pattern registration method to overcome the problems of spatial normalization of PET visualization data. Page 1472 Fda Approval of Diagnostic Drugs: Gorovets and colleagues review specific approved diagnostic radiopharmacetics to illustrate the ways in which imaging performance is characterized in clinical trials, and the clinical usefulness of imaging information included in drug labels. Page 1479 Heart Spectre/CT and PET/CT 1.0: Dorbala and fellow experts from SNMMI, ASCC, and SCCT provide the full text of the latest joint guidelines on cardiac SPECT/CT and PET/ Page 1485 Page 3 J Nucl Med August 1, 2013 volume 54 No 8 1512 Correction in Seo and others. etc. Full Text (PDF) Download citing article information Quoting articles via Google Scholar Search for related content Download information about related web page Page 4 4